Folding and Assembly of Dimeric Human Glutathione Transferase A1-1[†]

Louise A. Wallace and Heini W. Dirr*

Protein Structure−Function Research Program, Department of Molecular and Cell Biology, University of the Witwatersrand, Johannesburg, 2050, South Africa

Received June 1, 1999; Revised Manuscript Received October 6, 1999

ABSTRACT: Glutathione transferases function as detoxification enzymes and ligand-binding proteins for many hydrophobic endogenous and xenobiotic compounds. The molecular mechanism of folding of urea-denatured homodimeric human glutathione transferase A1-1 (hGSTA1-1) was investigated. The kinetics of change were investigated using far-UV CD, Trp20 fluorescence, fluorescence-detected ANS binding, acrylamide quenching of Trp20 fluorescence, and catalytic reactivation. The very early stages of refolding (millisecond time range) involve the formation of structured monomers with nativelike secondary structure and exposed hydrophobic surfaces that have a high binding capacity for the amphipathic dye ANS. Dimerization of the monomeric intermediates was detected using Trp fluorescence and occurs as fast and intermediate events. The intermediate event was distinguished from the fast event because it is limited by a preceding slow trans-to-cis isomerization reaction (optically silent in this study). At high concentrations of hFKBP, dimerization is not limited by the isomerization reaction, and only the fast event was detected. The fast ($\tau = 200$ ms) and intermediate ($\tau = 2.5$ s) events show similar urea-, temperature-, and ionic strength-dependent properties. The dimeric intermediate has a partially functional active site (∼20%). Final reorganization to form the native tertiary and quaternary structures occurs during a slow, unimolecular, urea- and ionic strength-independent event. During this slow event ($\tau = 250$ s), structural rearrangements at the domain interface occur at/near Trp20 and result in burial of Trp20. The slow event results in the regain of the fully functional dimer. The role of the C-terminus helix 9 (residues 210−221) as a structural determinant for this final event is proposed.

The molecular mechanisms of protein folding, i.e., how the primary amino acid sequence directs the rapid formation of the functional three-dimensional native state (*1*), have been extensively studied (*2*−*4*). The folding mechanisms of simple monomeric protein systems have been extensively studied (*4*). These studies, while important for our understanding of the role of intramolecular forces in folding and stabilizing secondary and tertiary structure, provide little information on how intermolecular associations stabilize oligomeric protein systems. The oligomeric nature of many proteins plays an essential role in determining their unique biological function in vivo. The folding pathways of some oligomeric proteins have been reported (for examples, see refs *5*−*10*).

In this study, the mechanism of folding of homodimeric human glutathione transferase A1-1 (hGSTA1-1)[1] was investigated. hGSTA1-1 is a member of the superfamily of cytosolic glutathione transferases (GSTs, EC 2.5.1.18). In the cell, the dimeric nature of GSTs enables them to function as part of the Phase II detoxification mechanism and as ligand-binding proteins (*11*). Cytosolic GSTs exist as homo- or heterodimeric structures ($M_r \sim 50\,000$) that are assembled from identical or nonidentical subunits from the same gene class. The cytosolic GSTs exhibit multiple enzyme forms that are grouped into seven species-independent gene classes (*12*−*16*). Crystal structures for the classes show that the overall polypeptide fold and topology are similar (*17*). Generally within each class there is a high sequence identity (>70%) while between the classes the identity is lower (20−30%).

Each subunit of GSTA1-1 consists of 221 amino acids each (Figure 1) and is composed of 2 structurally distinct domains with well-conserved cores: a small thioredoxin-like N-terminal alpha/beta domain (domain I) and a larger all-alpha-helical domain (domain II). The C-terminus (helix 9) forms part of the hydrophobic electrophile-binding site in domain I. This structural feature, unique to the alpha class GSTs, shows conformational heterogeneity in the absence/presence of ligands (*18, 19*). GSTs exist as functional dimers with one active site per subunit. Class-specific molecular recognition involves primarily interactions between domain I of the one subunit with domain II of the other subunit. The dimerization results in formation of an amphipathic cleft at the dimer interface which is postulated to bind nonsubstrate ligands (*20*−*22*).

Thermodynamic (un)folding studies have been reported for various members of the GST superfamily (*23*−*28*).

[†] This work was supported by the University of the Witwatersrand, the South African National Research Foundation, and the Alexander von Humboldt Foundation.

* To whom correspondence should be addressed. E-mail: 089dirr@cosmos.wits.ac.za. Fax: +27 11 403 1733.

[1] Abbreviations: ANS, 8-anilino-1-naphthalenesulfonate; CD, circular dichroism; hFKBP, human FK-binding protein; hGSTA1-1, human class alpha glutathione transferase with two type-1 subunits; k_f, second-order rate constant for folding; K_{sv}, collisional quenching constant (Stern−Volmer constant); NATA, *N*-acetyl-L-tryptophanamide; SASA, solvent-accessible surface area; Sj26GST, *Schistosoma japonicum* class mu glutathione transferase with two 26 kDa subunits; τ, time constant (inverse of the rate constant).

10.1021/bi991239z CCC: $18.00
Published on Web 11/24/1999

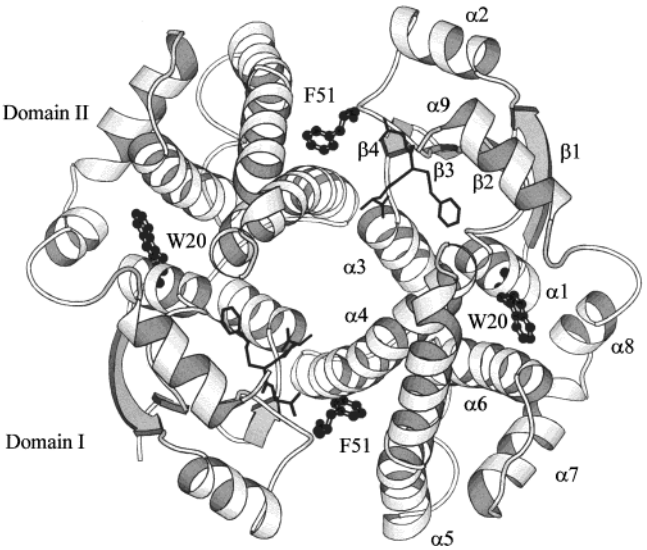

FIGURE 1: Schematic representation of dimeric GSTA1-1 parallel to the 2-fold axis. The active site ligand *S*-benzylglutathione and helix 9 structured over domain I are indicated. The secondary structural elements are labeled for clarity. The single tryptophan (Trp20) per subunit and the lock-and-key motif at the dimer interface involving Phe51 are shown. The figure was generated using MOLSCRIPT (*48*) from crystallographic coordinates (*41*).

hGSTA1-1 unfolds via a three-state kinetics pathway in which only the folded dimer and unfolded monomer are significantly populated at equilibrium; a nativelike transient dimeric intermediate with partially dissociated domain I and domain II was detected using stopped-flow kinetics (*26*). In addition, a topologically conserved bulky aliphatic residue (Leu164 in helix 6) plays a role in stabilizing and specifying the hydrophobic core of domain II and the interface of domains I and II (*27*).

In this paper, the first kinetics folding model for the glutathione transferase supergene family will be reported. Folding of GSTA1-1was investigated using far-UV CD, intrinsic Trp fluorescence, quenching of Trp20 fluorescence by acrylamide, fluorescence-detected binding of the amphipathic dye ANS, and catalytic reactivation. GSTA1-1 folds rapidly (milliseconds) to form structured monomers with loosely packed and exposed hydrophobic clusters/cores. Subunit association, domain docking, and the formation of a fully active folded dimer follow these early events.

MATERIALS AND METHODS

Reagents. Ultrapure urea was purchased from ICN Biomedicals; ultrapure acrylamide and α-chymotrypsin were from Boehringer Mannheim. ANS and the synthetic peptide *N*-succinyl-Ala-Ala-Pro-Phe-*p*-nitroanilide were purchased from Sigma. The Ex-Site mutagenesis kit was from Stratagene, and the restriction enzymes were purchased from Amersham Life Science. FK506 was a gift from Fujisawa Pharmaceutical Co., Ltd., Japan. Purified hFKBP was a generous gift from Jens-U Rahfeld and Gunter Fischer (*29*). All other reagents were of analytical grade.

Plasmids and Mutagenesis. The plasmid pKHA1, encoding the cDNA for GSTA1-1, was a gift from Prof. B. Mannervik (*30*). Site-directed mutagenesis to create a9delGSTA1-1 (truncated from residue 210) was performed by combining inverse PCR with long PCR to introduce the mutation directly into an intact plasmid template (*31*; Ex-Site mutagenesis kit).

Protein Purification. GSTA1-1 was purified using *S*-hexylglutathione affinity chromatography (*18, 32*) and eluted as previously described (*26*). Because of the reduced affinity of the mutant protein for the *S*-hexylglutathione affinity matrix, the protein was purified using CM-Sephadex cation exchange chromatography. The column was preequilibrated with 10 mM sodium phosphate buffer, pH 7.0, and the protein was eluted using a 0−0.5 M NaCl gradient. The mutant protein eluted at approximately 0.3 M NaCl, and the GST-containing samples were buffer-exchanged into 20 mM sodium phosphate buffer, pH 6.5, containing 0.1 M NaCl and 1 mM EDTA. The purity of the mutant protein, as judged by Coomassie-stained SDS−PAGE (*32*) and SEC−HPLC, was greater than 95%. The protein concentration of the dimer was estimated spectrophotometrically using a molar extinction coefficient of 38 200 M^{-1} cm^{-1} at 280 nm.

Reactivation Measurements. The activity of GSTA1-1 was determined spectrophotometrically at 340 nm in 0.1 M potassium phosphate buffer, pH 6.5, containing 1 mM CDNB, 3% (v/v) ethanol, and 1 mM reduced GSH (*33*). Six micromolar hGSTA1-1 denatured in 6 M urea was refolded by dilution (1:5) to 1 or 3 M urea at 15 °C. The regain in activity was determined by assaying 10 μL aliquots of refolded enzyme at room temperature (∼21 °C). Approximately 15−20% reactivation occurred within the dead time (∼18 s) of the measurements.

Denaturation/Renaturation of hGSTA1-1. hGSTA1-1 (0.3−30 μM) was denatured at room temperature (25 °C) for at least 1 h in 6 M urea (20 mM sodium phosphate, pH 6.5, containing 1 mM EDTA and 0.1 M NaCl). Refolding was initiated by dilution of denatured protein (1:5 asymmetric mixing) with the sodium phosphate buffer. Refolding kinetics were assessed under a variety of conditions: (1) denaturant dependence (1−4.25 M urea); (2) protein concentration dependence (0.5−3 μM) at 1 M urea; (3) ionic strength dependence (0−1 M NaCl) at 1 M urea; and (4) temperature dependence (5−40 °C) at 1 M urea. Catalysis of refolding by peptidyl-prolyl isomerase at 1 M urea was investigated using increasing amounts of hFKBP (0−6 μM). hFKBP was included in the refolding buffer. Inhibition of isomerase activity was carried out with final concentrations of 40 μM FK506 and 4 μM hFKBP. Refolding of 6 μM GSTA1-1 denatured in 6 M urea was also determined in the presence of either 167 μM ANS or 0.12 M acrylamide (the reagents were included in the refolding buffer). For refolding in the presence of acrylamide, parallel runs were performed in the absence (F_o) and presence (F) of acrylamide.

Stopped-Flow Fluorescence. The change in fluorescence upon refolding was monitored using an Applied Photophysics (SX-18MV) stopped-flow analyzer. Excitation was at 280 nm and emission monitored above 320 nm using a cutoff filter. Excitation and emission path lengths were 10 and 2 mm, respectively, and the excitation band-pass was 2.32 nm to minimize photodecomposition. Refolding in the presence of ANS was monitored by excitation at 350 nm and emission greater than 400 nm. The dead time of the instrument was determined to be 2 ms (*34*). Typically, 3−4 kinetic runs were averaged, and the standard deviation was calculated from at least three separate experiments. The temperature was

regulated within 0.1 °C of the required temperature using a thermostated water bath.

Various control experiments established that the refolding events observed were real and not the result of aggregation or mixing artifacts. The absence of aggregation was confirmed by monitoring absorbance at 340 nm. In addition, control refolding experiments using NATA and *N*-acetyl-L-tyrosinamide confirmed the absence of mixing artifacts. Control runs (buffer/buffer, buffer/urea, buffer/protein) showed a horizontal signal response.

Stopped-Flow Far-UV CD. The change in ellipticity upon refolding was monitored using the Applied Photophysics CD-spectra kinetic accessory (CD.2C) interfaced to the stopped-flow apparatus. Ellipticity was monitored at 226 nm using a path length of 2 mm and slit widths of 0.5 and 1 mm for monochromators 1 and 2, respectively. The CD signal was calibrated using 1 mg/mL (1*S*)-(+)-10-camphorsulfonic acid. The dead time of the instrument was determined to be 10 ms (*34*). For CD measurements, 20 μM protein in 6 M urea was diluted 6-fold to a final urea concentration of 1 M at 15 °C. The final protein concentration was 3.3 μM. A total of 15−20 kinetic runs were averaged per experiment, and the raw CD signal was normalized by calculation of the mean residue ellipticity.

Data Analysis. All kinetic refolding traces were analyzed using the Applied Photophysics software v.4.24/v4.36. The deviation of the fitted function from the experimental data (i.e., the residuals) was used to judge the quality and accuracy of the fit. The manner of determining the rate constants is reported in the figure legends.

The temperature dependence of the refolding rates was analyzed using the Arrhenius theory [$k = A \exp(E_A/RT)$]. The ionic strength dependence of the refolding rate was related to the electrostatic component of the mean rational activity coefficient. The mean rational activity coefficient was analyzed using an extension of the Debye−Hückel theory for a 1:1 electrolyte, developed by Koppenol (*35*) as described (*36*).

The SEM values reported are for the least-squares fitting of the data to the appropriate equation (Sigma Plot, v 5.0; Jandel Corp.).

RESULTS

The structure as well as the catalytic and ligand-binding functions of GSTA1-1 are reversibly (>90%) perturbed by urea denaturation (*26*). Refolding and assembly of the homodimeric GSTA1-1 were studied by dilution of urea-denatured protein into refolding buffer containing different concentrations of urea. Considering the complexity of the GST molecule, a variety of probes were necessary to monitor changes at different structural levels during the refolding process.

Far-UV CD-Detected Refolding. According to the crystal structure of the uncomplexed enzyme (*18*), the hGSTA1-1 polypeptide is about 56% alpha-helical. This is reflected in the far-UV CD spectrum for folded hGSTA1-1 that exhibits two ellipticity minima at 208 and 222 nm, and the secondary structure is completely disrupted as the protein unfolds (at urea concentration greater than 6 M; inset of Figure 2). Refolding kinetic traces show that a significant proportion of the negative ellipticity at 226 nm was acquired in the dead time of the instrument (Figure 2); the burst phase amplitude of the reaction measured was approximately 75−80% at 1 M urea. The appearance of a high percentage of native ellipticity in the burst phase indicates that substantial native helical secondary structure is rapidly formed during refolding.

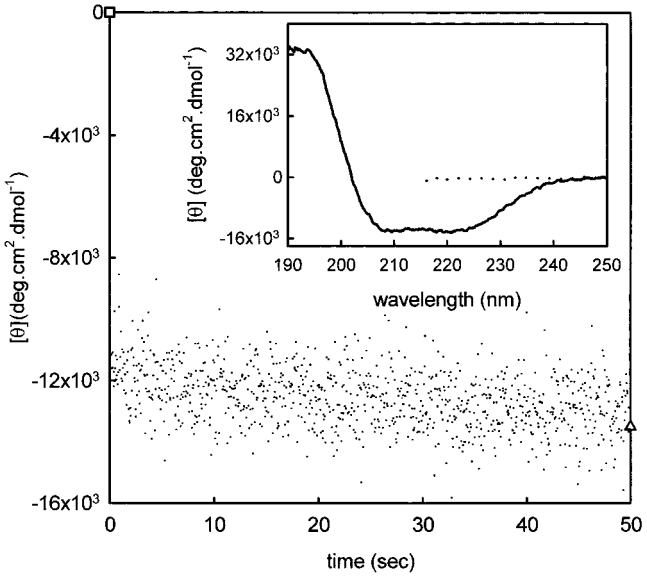

FIGURE 2: Kinetics of refolding of urea-denatured GSTA1-1 monitored using far-UV CD at 226 nm. Final conditions: 1 M urea, 3.3 μM protein, 15 °C, 0.1 M NaCl. The initial (□) and final (△) ellipticity values for denatured and native protein, respectively, are indicated. Inset: far-UV CD spectra for 1 μM native GSTA1-1 (solid line) and 1 μM GSTA1-1 in 9 M urea (dotted line).

Intrinsic Trp Fluorescence. Its single tryptophan residue (Trp20) per subunit dominates the intrinsic fluorescence emission properties of GSTA1-1 (*26*). Trp20 is located in helix 1 of domain I, and its indole side chain protrudes into domain II (Figure 1). Therefore, Trp 20 should be sensitive to structural changes occurring at/near the domain−domain interface (*19, 26*). The fluorescence intensity of Trp20 in GSTA1-1 is quenched in the unfolded state possibly as a result of collisional quenching with the protonated side chain of the neighboring Arg19. Refolding kinetics of hGSTA1-1 were monitored using Trp fluorescence over a wide range of denaturant concentration (1−4.5 M urea), protein concentration (0.5−3 μM), temperature (5−40 °C), and ionic strength (0−1 M NaCl). Kinetic traces could be resolved into three distinct phases (Figure 3): fast, intermediate, and slow phases. During the fast and intermediate refolding phases, there is an increase in fluorescence to a value greater than the native fluorescence signal (Figure 3). The native value is gained during the slow phase which displays reverse polarity (inset of Figure 3). At 1 M urea (15 °C), the time constants for the fast, intermediate, and slow phases are approximately 200 ms, 2.5 s, and 250 s, respectively. The initial and final amplitudes are as predicted from equilibrium studies with no burst phase observed.

Figure 4 shows a linear urea dependence of the apparent refolding rates at 15 °C. The three distinct phases were observed at all denaturant concentrations. The rate constants for the fast and intermediate phases decrease as the concentration of denaturant increases whereas the rate constant for the slow phase appears to be denaturant-independent. The linear dependence of the refolding rate on denaturant for the fast ($r = 0.992$) and the intermediate ($r = 0.988$) phases

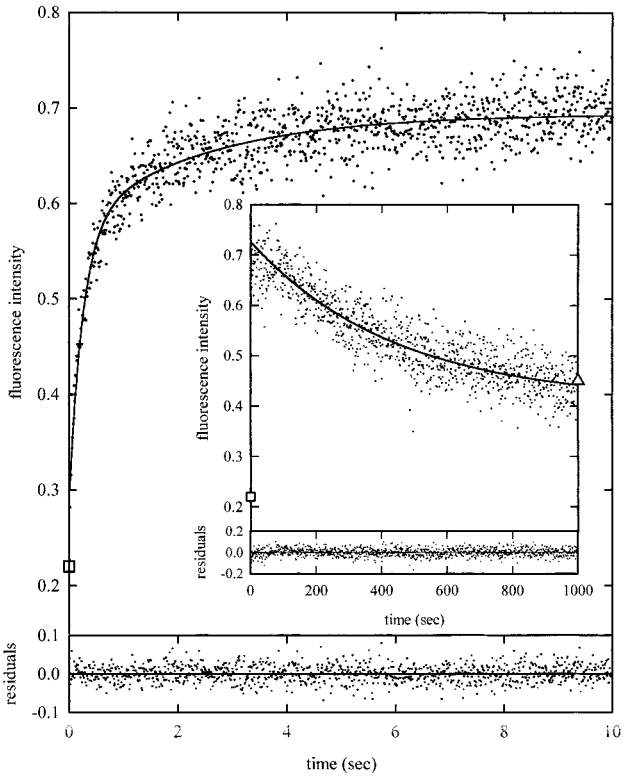

FIGURE 3: Kinetics of refolding of urea-denatured GSTA1-1 monitored by Trp fluorescence (ex 280 nm, em >320 nm). Final conditions: 1 M urea, 1 μM protein, 15 °C, 0.1 M NaCl. The fast and intermediate phases (best fit to a biexponential function) and the slow phase (inset, best fit to a single exponential) are shown. The residuals for the fit are indicated in the lower panel of each trace. The initial (□) and final (△) amplitude values for denatured and native protein, respectively, are indicated.

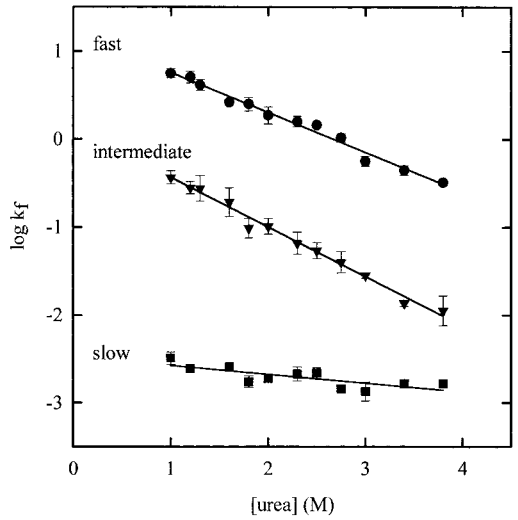

FIGURE 4: Urea dependence of the refolding rate constant (k_f) for the fast (●), intermediate (▼), and slow (■) phases, measured by Trp fluorescence (ex 280 nm, em >320 nm). Final conditions: 1 μM protein, 15 °C, 0.1 M NaCl. The solid lines are the best fit to a linear function. The error bars are as indicated or are comparable to the size of the symbol.

suggests no changes in the rate-limiting steps. The parallel slopes observed for the denaturant-dependent behavior of the fast (m_f = 263.8 cal mol^{-1} M^{-1}) and intermediate (m_f = 323.0 cal mol^{-1} M^{-1}) phases suggest similar compactness (i.e., solvent accessibility) of the transition states for these phases. The rate constant of the third and slowest phase showed a weak denaturant dependence (m_f = 57.0 cal mol^{-1} M^{-1}).

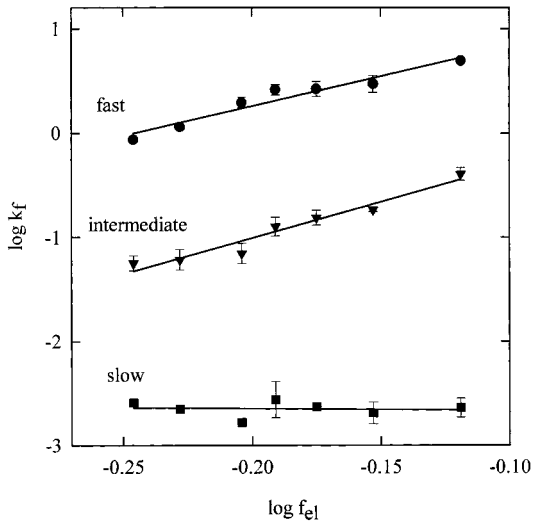

FIGURE 5: Ionic strength dependence of the rates of refolding (k_f) for the fast (●), intermediate (▼), and slow (■) phases, measured using Trp fluorescence (ex 280 nm, em >320 nm). Final conditions: 1 M urea, 1 μM protein, 15 °C. The solid lines are the best fits to log k_f = log k (I = 0) + α log f_{el} (*36*).

The urea dependence of the amplitudes for the refolding events indicates that the fast, intermediate, and slow phases account for 37%, 22%, and 40% of the expected total amplitude change, respectively (see Figure 4b in *26*).

Both the fast and the intermediate phases proceed more rapidly at higher protein concentrations at 15 and 25 °C and at 1 and 3 M urea (not shown) and in the presence of acrylamide (see below), suggesting a bimolecular (second-order) rate-limiting step for each event. Values for the second-order refolding rate, k_f (k_{app} = 4k_f[P$_t$]; *8*), were estimated to be 4.8 × 10^5 (±1.6 × 10^5) M^{-1} s^{-1} and 2.8 × 10^4 (±8.7 × 10^3) M^{-1} s^{-1} for the fast and intermediate phases at 1 M urea, 15 °C (not shown). The slow phase, however, exhibited a weak protein concentration dependence [k_f = 58.8 (±13.0) M^{-1} s^{-1}; not shown] and is most likely unimolecular.

The temperature dependence (5−40 °C) of the three refolding phases was investigated at 1 M urea (not shown). The apparent refolding rate for the fast phase increases at 40 °C such that 50% of the reaction occurs as a burst phase. The refolding rates for all three phases were best described using a linear Arrhenius function. The linear dependence is different from that observed for the refolding of a large number of proteins and suggests small heat capacity differences between the set of intermediates and the rate-limiting transition states. Values for activation energy were 8.50, 9.50, and 15.08 kcal/mol for the fast, intermediate, and slow phases, respectively.

The effects of ionic strength on the refolding rates of the fast, intermediate, and slow phase are illustrated in Figure 5. The three phases have amplitudes similar to those detected in the absence of salt. However, salt significantly decreased the apparent rates of refolding of the fast and intermediate phases, suggesting that specific ionic interactions are formed during these events which are screened by salt. Furthermore, the parallel slopes for the salt dependence suggest that the ionic interactions formed during the fast and intermediate phases are very similar and the linear correlation between

log k_f and log f_{el} is consistent with formation of favorable ionic interactions between the associating molecules (*36*). The slow refolding phase is, however, essentially salt-insensitive (Figure 5). Control CD measurements indicate that the helical content of GSTA1-1 was unaffected by the presence of 1 M NaCl (data not shown).

Trp20 Fluorescence Quenching by Acrylamide. Quenching of tryptophan fluorescence by the neutral polar collisional quencher acrylamide is very sensitive to changes in the fluorophore's environment and thus provides a measure of the burial of tryptophans as a protein folds (*37*). In the native folded GSTA1-1, Trp20 is largely inaccessible to solvent ($\lambda_{max} = 325$ nm; SASA = 4 Å^2; $K_{sv} = 2.19$ M^{-1}). However, upon unfolding of GSTA1-1, Trp20 becomes accessible to solvent ($\lambda_{max} = 355$ nm; $K_{sv} = 13$ M^{-1}). A linear Stern−Volmer plot ($F_o/F = 1 + K_{sv}$[acrylamide] (*38*), with quencher concentrations <0.2 M) for folded GSTA1-1 indicates that the single Trp residue per subunit is equally accessible to solvent. As urea-denatured GSTA1-1 refolds, the exclusion of the indole side chain of Trp20 from the polar solvent should be reflected by a decrease in the ease at which acrylamide encounters the residue.

The change in solvent accessibility of Trp20 as denatured GSTA1-1 refolds was investigated at 1 M urea, 15 °C, in the presence of a final concentration of 0.12 M acrylamide. The extent of fluorescence quenching is described as F_o/F, which is the ratio of the fluorescence intensity in the absence of quencher to that in the presence of quencher. An F_o/F versus time trace for the refolding of GSTA1-1 is represented in Figure 6. The change in F_o/F is triphasic; i.e., the sequestration of Trp20 occurs in three successive phases with time constants of 170 ms (fast phase), 2.9 s (intermediate), and 250 s (slow); 30% of the fast phase occurs in the dead time. The fast [$k_f = 5.7 \times 10^5$ ($\pm 3.5 \times 10^4$) M^{-1} s^{-1}] and intermediate [$k_f = 4.7 \times 10^4$ ($\pm 1.3 \times 10^3$) M^{-1} s^{-1}] phases proceeded more rapidly at higher protein concentrations (data not shown). Therefore, the sequestration of Trp20 from solvent parallels the changes detected using intrinsic fluorescence. These data indicate that the tertiary environment and solvent accessibility of Trp20 are not fixed until the last events of folding.

Agreement of the refolding data using intrinsic fluorescence and solvent accessibility as probes and control experiments (which indicate that low concentrations of acrylamide have no effect on GSTA1-1 activity/regain in activity) suggest that acrylamide does not perturb the last refolding events or alter the stability of any of the folding intermediates.

Fluorescence-Detected ANS Binding. The amphipathic fluorescent probe ANS has been extensively used to monitor the formation of hydrophobic cores/clusters during protein folding (*39*, *40*). ANS binds to the folded state of GSTA1-1 with an apparent dissociation constant of 16 μM. On binding GSTA1-1, its fluorescence is significantly enhanced, and its emission maximum wavelength shifts from 530 nm (in water) to 475−485 nm (indicative of a nonpolar environment). The dye was proposed, using fluorescence resonance energy transfer, to bind in the nonsubstrate ligand-binding site at the dimer interface formed by subunit association (*21*, *22*).

The refolding of GSTA1-1 as detected by ANS binding is shown in Figure 7. There is an initial rapid enhancement of ANS fluorescence relative to free ANS, and the increase

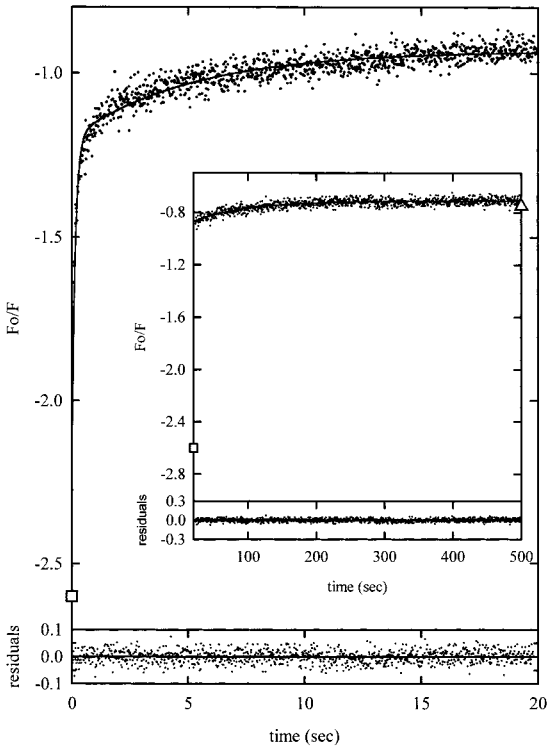

FIGURE 6: Kinetics of refolding of urea-denatured GSTA1-1 in the presence of 0.12 M acrylamide monitored by Trp fluorescence (ex 280 nm, em >320 nm). The extent of fluorescence quenching (F_o/F) is shown as a function of time. Residuals for the fit to a biexponential (over 20 s) and a single-exponential function (>20 s, inset) are shown (lower panel). The initial (□) and final (△) values for F_o/F are shown. Final conditions: 1 M urea, 1 μM protein, 15 °C, 0.1 M NaCl.

continues up to 10 ms (inset of Figure 7). The substantial increase in the fluorescence intensity of ANS (~600%) within the burst phase suggests preferential binding of ANS to some partially folded and loosely packed intermediate with exposed hydrophobic patches (molten globule-like). The enhancement is followed by a rapid decrease in fluorescence (single exponential, $\tau = 100$ ms) signifying desorption of ANS as a consequence of substantial burial of hydrophobic surfaces and structural rearrangements. Thereafter, the fluorescence intensity decreases in a biphasic manner ($\tau =$ 60 and 290 s). The final fluorescence intensity, as predicted by equilibrium studies, is enhanced (~300%) relative to free ANS. This most likely represents ANS bound at the subunit interface of the nativelike dimeric state (Figure 7). Equilibrium and kinetic unfolding studies have shown that ANS does not bind the unfolded state of GSTA1-1 and does not alter the conformational stability and unfolding kinetics (*26*, unpublished data). In addition, the rate constants for the various phases are independent of the final concentration of ANS (data not shown). However, because of the different time constants observed, it was not possible to conclude that ANS does not perturb the refolding of A1-1, and hence interpretation of the data is limited to a description of the burst phase.

Refolding Measured by Activity. The basic structural framework of the active site for GSTs is formed by domain I of each subunit. In addition, the formation of a fully active dimer of GSTA1-1 is dependent on interactions from domain I from one subunit and two amino acid residues (Asp100 and Arg130) from domain II of the other subunit (*17*). The

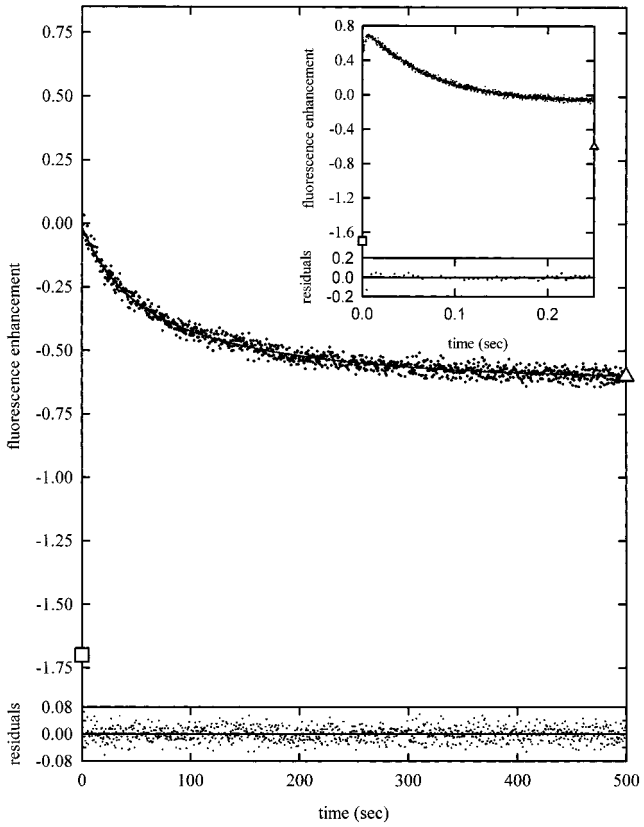

FIGURE 7: Kinetics of refolding of urea-denatured GSTA1-1 in the presence of 167 μM ANS (ex 350 nm, em >400 nm). The burst phase and desorption of ANS (fitted to a single-exponential function) (inset) and the subsequent biphasic decrease are shown. Residuals are shown in the lower panel. Final conditions: 1 M urea, 1 μM protein, 15 °C, 0.1 M NaCl. The initial fluorescence intensity of free ANS (□) and the final fluorescence intensity for ANS bound to GSTA1-1 in 1 M urea (△) are shown.

dissociation and unfolding of GSTA1-1 result in a complete loss in activity (*26*).

The regain of activity of GSTA1-1 during refolding was accompanied by a 15−20% burst phase within 18 s. Refolding to 1 M urea resulted in a fully active dimer (∼100%) within 120 s at 21 °C; the recovery of activity was too fast to measure its time dependence manually with a reasonable degree of accuracy. Refolding to 3 M urea resulted in 15−20% recovery of activity in 18 s (the dead time of mixing), and ∼65% of the activity was regained within 600 s (not shown). Refolding to 3 M urea resulted in only 85% regain in activity and was best described using a single-exponential function ($r^2 = 0.90$) where $\tau = 250$ s.

Role of cis/trans Isomerization in Refolding of GSTA1-1. GSTA1-1 has 10 proline residues per subunit, and the peptide bond preceding Pro55 is in the cis configuration in the native folded state (*41*). This cis-Pro motif, located between helix 2 and strand 3 in domain I, is conserved in all GSTs (*17*) and is postulated to maintain the correct conformation of the active site (*42*).

hFKBP, a peptidyl-prolyl isomerase (*43*), was used to detect whether any of the refolding phases of GST A1-1, detected using Trp fluorescence, are limited by proline isomerization. The effect of increasing concentrations of hFKBP on the refolding rates is shown in Figure 8. The rate constant of the fast phase was unaffected and the slow phase weakly affected while the rate constant for the intermediate

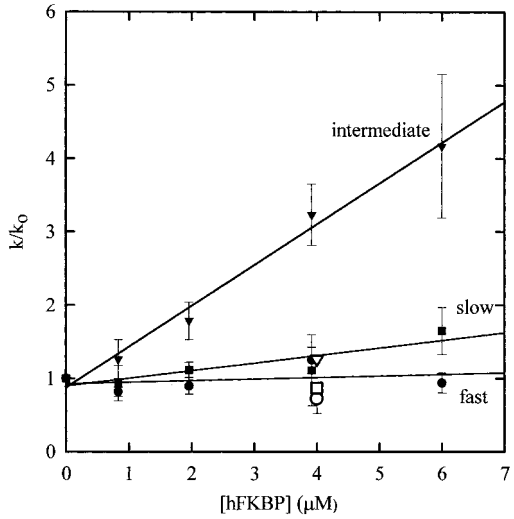

FIGURE 8: Catalytic effect of hFKBP on the rates of refolding of the fast (●), intermediate (▼), and slow (■) phases of urea-denatured GSTA1-1. Final conditions: 1 M urea, 1 μM protein, 15 °C, 0.1 M NaCl. The ratio of k/k_o was calculated from the refolding rate in the presence (k) and the absence (k_o) of hFKBP. Error bars are as indicated. The inhibition of 4 μM hFKBP activity by 40 μM FK506 for the fast (○), intermediate (▽), and slow (□) phases is indicated.

phase was accelerated approximately 5-fold in the presence of 6 μM hFKBP. The relative amplitudes were approximately the same as those in the absence of the catalyst. At high concentrations of hFKBP, the refolding traces of the fast/intermediate phases were still best fit to a biexponential function although the differences between the single and biexponential fits became less discernible. Catalysis of the intermediate phase by hFKBP was eliminated when 40 μM FK506, an inhibitor of the prolyl isomerase activity of hFKBP, was included in the refolding buffer (Figure 8).

Refolding of a9delGSTA1-1. The role of helix 9 (residues 210−221 at the C-terminus) in the folding pathway of GSTA1-1 was investigated using a truncated form of the enzyme. The truncation had little impact on the gross structural properties of GSTA1-1 and no overall effect on the fluorescence-detected equilibrium and kinetic unfolding pathway. Therefore, any changes in the refolding pathway should be the consequence of the absence of the C-terminal region of the GST A1 polypeptide.

The refolding kinetic traces for a9delGSTA1-1 to 1 M urea, 15 °C, monitored using intrinsic Trp fluorescence (Figure 9) and quenching by acrylamide (data not shown) were triphasic. The Trp fluorescence kinetic trace was resolved into three phases with time constants of 330 ms (fast), 8 s (intermediate), and 160 s (slow). The time constants for the fast and intermediate phases are similar to those reported for the wild-type protein; however, the time constant for the slow event is much reduced. Furthermore, the reversed polarity of the fluorescence intensity observed for the slow phase for wild-type GSTA1-1, using Trp fluorescence, was not detected (see inset of Figure 9 compared with inset of Figure 3). The native final value for refolding was gained during the slow phase.

Biochemical Characterization of Refolded GSTA1-1. The physiochemical properties of refolded GSTA1-1 to 1 M urea were compared with those for native GSTA1-1 in 1 M urea. Far-UV CD and steady-state emission spectra indicate that

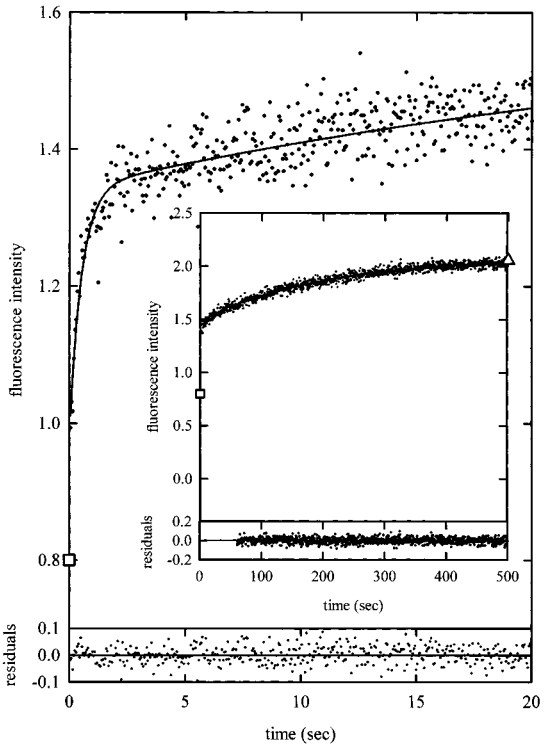

FIGURE 9: Kinetics of refolding of urea-denatured a9delGSTA1-1 monitored by Trp fluorescence (ex 280 nm, em >320 nm). Final conditions: 1 M urea, 1 μM protein, 15 °C, 0.1 M NaCl. Residuals for the fit to a biexponential (fast and intermediate phases over 20 s) and a single-exponential function (>20 s, slow phase inset) are shown (lower panel). The initial (□) and final (△) amplitude values are as indicated.

the secondary (similar ellipticity values) and tertiary (similar intensities and maximum emission wavelength) structures of refolded A1-1 are indistinguishable from those of native GSTA1-1. In addition, urea SEC−HPLC shows that the overall hydrodynamic volume is unchanged at 0 and 1 M urea (data not shown). Activity measurements are consistent with the reactivation data (see above) and indicate that GSTA1-1 refolded to 1 M urea is 100% active. Stern−Volmer constants (K_{sv}) calculated from acrylamide quenching studies (data not shown) using refolded protein indicate that the solvent accessibility of Trp20 is similar at 1 M urea (K_{sv} = 1.97 M^{-1}) to that in the absence of urea (K_{sv} = 2.19 M^{-1}).

DISCUSSION

The kinetics folding pathway for hGSTA1-1 reported here is the first proposal of a folding and subunit assembly model for the glutathione transferase superfamily. The high levels of structural organization of the GSTs and the wealth of structural information available (for review, see ref *17*) provide insight into the role of interdomain and intersubunit interactions in stabilizing and specifying the native dimeric state. The kinetic refolding pathway of dimeric GSTA1-1 is more complex than the minimal two-state model where unstructured monomers collide to form the native folded state, in a single phase.

Folding Scheme for GSTA1-1. Our studies with GSTA1-1 reveal the transient formation of a number of partially folded species. A sequential and parallel refolding pathway is proposed based on experimental and structural evidence: see Scheme 1, where U denotes unfolded conformers and the

Scheme 1

$$\begin{array}{ccccccc} 2U_c & \rightarrow & 2M_c & \rightarrow & N_2^* & \rightarrow & N_2' \rightarrow N_2 \\ \updownarrow & & & & \uparrow & & \\ 2U_t & \rightarrow & 2M_t & & & & \end{array}$$

subscripts c and t represent the cis/trans isomers of the X−Pro peptide bond, M represents folded monomers with nativelike secondary structure and loose hydrophobic packing, N_2* is a dimeric intermediate with the native configuration about the peptide bonds but with a coillike conformation for helix 9, and N_2' and N_2 are folded dimeric states with helix 9 structured yet mobile for N_2' and structured and packed against domain I for N_2.

Formation of Monomers Precedes Association. The earliest events, detected as a burst phase (less than 10 ms), resulted in the formation of monomeric intermediates (2U→2M; Scheme 1) with secondary structural content very similar to that of the native protein. Furthermore, the monomeric states are compact with a significant amount of exposed hydrophobic surface. The structural properties of the transient monomeric state(s) resemble those of the equilibrium molten-globule state observed for a number of proteins; i.e., it has intact secondary structure with ill-defined tertiary structure and displays a high capacity for the amphipathic dye ANS. It is the absence of rigid tertiary packing of hydrophobic clusters that makes the hydrophobic core more accessible to solvent. Intermediates with similar characteristics have been described during the burst phase of refolding for several proteins (*3*, *40*). In general, it is not clear whether secondary structure formation accompanies the formation of hydrophobic cores/clusters or not. The early folding events for GSTA1-1 occur prior to formation of fixed native tertiary structural elements and indicate that specific intramolecular interactions are formed rapidly and do not act as rate-limiting steps for the overall folding reaction of GSTA1-1. Under the conditions of this study, the reactions $2U_c \rightarrow 2M_c$ and $2U_t \rightarrow 2M_t$ were spectroscopically indistinguishable (Scheme 1).

Formation of Dimeric Intermediates. The $2M \rightarrow N_2$* dimerization reaction (Scheme 1) was detected during the fast and intermediate events. The intermediate event is limited by a preceding slow isomerization reaction, $2M_t \rightarrow 2M_c$ (optically silent in this study). At high concentrations of hFKBP, dimerization is no longer limited by trans-to-cis proline isomerization, and hence only the fast event was detected.

The large second-order rate constant values for both the fast and intermediate phases is consistent with the productive interaction of a large fraction of preassembled monomers formed early in the folding pathway (see above) (*8*). Furthermore, the transition state properties for the fast and intermediate phases display a number of interesting features. First, the folding rates for both phases show a weak dependence on the denaturant, suggesting that the transition state occurs early in the folding pathway and that the ensemble of molecules at the transition state are largely accessible to solvent. Second, the urea/temperature/ionic strength dependence of the intermediate phase parallels that of the fast phase, suggesting that both populations of species occupy similar positions on the reaction coordinate diagram. These similar refolding properties indicate that the fast and intermediate events are monitoring the same folding reaction.

Catalysis of the intermediate event by hFKBP indicates that the event includes both an isomerization reaction as well as an association reaction. The isomerization most likely involves the cisVal54−Pro55 peptide bond. Because catalysis of the isomerization reactions depends on the accessibility of the reaction site and because the specificity for dimerization of GSTs is very stringent (see below), it is reasonable to expect that the isomerization event would occur prior to dimerization. The C-terminal truncated protein a9delGSTA1-1 refolds in a manner similar to the wild-type protein, indicating that helix 9 has little or no structural role during the association events and its conformation is coillike. Helix 9 is therefore not packed against domain I in the monomeric intermediate, making the region above the Val−Pro bond accessible to hFKBP.

Structural features at the subunit interface of GSTs indicate that molecular recognition at the dimer interface is strictly class-specific. The hydrophobic effect is the main driving force for the dimerization with about 16% of the solvent-accessible surface area being buried during dimerization (*41*, see also ref *44*). Hydrophobic and polar interactions between domain I of the one subunit and domain II of the other subunit stabilize and specify subunit association (*17*, *45*). The major hydrophobic interactions occur at either end of the dimer interface. In the alpha/mu/pi GSTs, a lock-and-key type hydrophobic interaction involving an aromatic residue (Phe51 in class alpha, see Figure 1) in domain I of the one subunit protrudes into a hydrophobic pocket in domain II of the neighboring subunit. In addition to the hydrophobic effect, prominent polar and charged interactions occur near the dimer 2-fold axis. The stacking of two symmetrically equivalent arginine groups (*17*) and a mixed charged cluster (*46*) creates much of the complementarity between the two surfaces, resulting in a curved topography for the subunit interface of the alpha/mu/pi GSTs. The high specificity and complementarity of subunit association requires that the loop between helix 2 and strand 3, on which the cis Val−Pro motif is located, be correctly orientated in order for dimerization to occur. It is therefore possible that the structuring of the loop region is dependent on the correct native peptide bond conformation and hence only those monomers with the correct cis configuration at Pro55 would associate. The ionic strength dependence of the refolding rate of the dimerization events, albeit modest, indicates that the electrostatic interactions formed during these events are important in orientating and positioning the appropriate surfaces between which the hydrophobic surfaces form and these two forces together stabilize the dimeric intermediate (*47*).

The association of the monomers results in the formation of a partially functional active site (approximately ~20% active). Furthermore, there is a substantial (biphasic) decrease in the capacity of the protein for ANS, reflecting the tighter packing of the hydrophobic core and structural reorganization. Concomitant with these events, there is further sequestration of Trp20 from solvent.

Final Structural Rearrangements. The final step in the refolding of GSTA1-1, detected using Trp fluorescence, is independent of urea and protein concentration and is insensitive to salt. This is consistent with the slow acquisition of a correctly assembled dimer (N_2*→N_2′). The absence of catalysis of this event by hFKBP suggests that this phase is not the consequence of isomerization reactions involving proline residues. It may be the result of isomerization of non-proline residues; however, it is feasible (see below) that the slow event arises from domain−domain/subunit−subunit rearrangements.

These structural rearrangements of the domain−domain/subunit−subunit interfaces are accompanied by the regain of a fully functional active site and complete burial of Trp20. The inverse amplitude (polarity) of the slow phase, detected using Trp fluorescence, is an interesting phenomenon. The location of Trp20 at the domain interface and the absence of a similar phenomenon during the refolding of a9delGSTA1-1 suggest that the properties of this event result from structural changes involving Trp20 and helix 9 (both of which are at/near the domain−domain interface; see Figure 1). Trp20 has been shown to be a useful probe for structural changes occurring at/near the domain interface (*19*, *26*). The indole side chain of Trp20 protrudes from domain I into domain II and has nonspecific hydrophobic contacts with the side chains of Ile157, Glu161, and Tyr164 (in helix 6) and Leu197 and Phe196 (in helix 8). Furthermore, a hydrophobic environment for Trp20 is created by the close packing on domain I of helix 8, the connecting segment between helices 8 and 9, and helix 9. The refolding of a9delGSTA1-1, detected using Trp fluorescence and acrylamide quenching studies, suggests that the structuring of helix 9 at the domain interface and its closure over domain I may retard the final folding event and hence the acquisition of native dimer. Furthermore, the structural dynamics of helix 9 in the absence/presence of ligand (*18*, *19*) suggest that in the absence of ligands, the helix is most likely structured but mobile (N_2′) while the presence of ligands causes the structured helix to be packed more tightly against domain I (N_2). The high cellular concentration of GSH (1−10 mM) suggests that the latter folded dimeric state is most likely to exist in vivo.

Implications of the Folding Scheme for the Glutathione Transferase Superfamily. From the proposed folding scheme for GSTA1-1, it is apparent that the higher order of organization of GSTs occurs as a final folding event and is essential for the enzymes to function in vivo as detoxification enzymes and ligand-binding proteins. This may have important implications in therapeutic studies since the role of GSTs in the transport and catalysis of xenobiotic compounds has resulted in these proteins being responsible for the acquisition of resistance toward a variety of xenobiotic compounds such as carcinogens, therapeutic agents, and pesticides (*47*).

The common fold and topology of this group of enzymes requires that the general applicability of the folding mechanism proposed above be investigated using other members of the family. These studies will provide information on how global properties, such as amino acid sequence, topology, and thermodynamic stability, can define the kinetics of oligomeric protein folding.

ACKNOWLEDGMENT

H.W.D is grateful to the Serrano group at EMBL, Heidelberg, Germany, for the use of their Jasco CD spectrophotometer during his sabbatical leave.

REFERENCES

1. Anfinsen, C. B. (1973) *Science 181*, 223−239.
2. Kim, P. S., and Baldwin, R. L. (1990) *Annu. Rev. Biochem. 59*, 631−660.
3. Matthews, C. R. (1993) *Annu. Rev. Biochem. 62*, 653−683.
4. Jackson, S. E. (1998) *Folding Des. 3* (4), R81−R91.
5. Ziegler, M. M., Goldberg, M. E., Chafotte, A. F., and Baldwin, T. O. (1993) *J. Biol. Chem. 268* (15), 10760−10765.
6. Mann, C. J., Shao, X., and Matthews, C. R. (1995) *Biochemistry 34*, 14573−14580.
7. Waldburger, C. D., Jonsson, T., and Sauer, R. T. (1996) *Proc. Natl. Acad. Sci. U.S.A. 93*, 2629−2634.
8. Wendt, H., Berger, C., Baici, A., Thomas, R. M., and Bosshard, H. R. (1995) *Biochemistry 34*, 4097−4107.
9. Munson, M., Anderson, K. S., and Regan, L. (1997) *Folding Des. 2* (1), 77−87.
10. Nichtl, A., Buchner, J., Jaenicke, R., Rudolph, R., and Scheibel, T. (1998) *J. Mol. Biol. 282*, 1083−1091.
11. Armstrong, R. N. (1991) *Chem. Res. Toxicol. 10*, 2−18.
12. Mannervik, B., Alin, P., Guthenberg, C., Jensson, H., Tahir, M. K., Warholm, M., and Jornvall, H. (1985) *Proc. Natl. Acad. Sci. U.S.A. 82*, 7202−7206.
13. Meyer, D. J., Coles, B., Pemble, S. E., Gilmore, K. S., Fraser, G. M., and Ketterer, B. (1991) *Biochem. J. 274*, 409−414.
14. Ji, X., von Rosenvinge, E. C., Johnson, W. W., Tomarev, S. I., Piatigorsky, J., Armstrong, R. N., and Gilliland, G. J. (1995) *Biochemistry 34*, 5317−5328.
15. Pemble, S. E., Wardle, A. F., and Taylor, J. B. (1996) *Biochem. J. 319*, 754−759.
16. Board, P. G., Baker, R. T., Chelvanayagam, G., and Jermiin, L. S. (1997) *Biochem. J. 328*, 929−935.
17. Dirr, H. W., Reinemer, P., and Huber, R. (1994) *Eur. J. Biochem. 220*, 645−661.
18. Cameron, A. D., Sinning, I., L'Hermite, G., Olin, B., Board, P. G., Mannervik, B., and Jones, T. A. (1995) *Structure 3*, 717−727.
19. Atkins, W. M., Dietze, E. C., and Ibarra, C. (1997) *Protein Sci. 6*, 873−881.
20. Reinemer, P., Dirr, H. W., Ladenstein, R., Schaffer, J., Gallay, O., and Huber, R. (1991) *EMBO J. 10*, 1997−2005.
21. Sluis-Cremer, N., Naidoo, N., Kaplan, W., Manoharan, T. H., Fahl, W., and Dirr, H. (1996) *Eur. J. Biochem. 241*, 484−488.
22. Sluis-Cremer, N., Wallace, L., Burke, J., Stevens, J., and Dirr, H. (1998) *Eur. J. Biochem. 257*, 434−442.
23. Dirr, H. W., and Reinemer, P. (1991) *Biochem. Biophys. Res. Commun. 180* (1), 294−300.
24. Erhardt, J., and Dirr, H. (1995) *Eur. J. Biochem. 230*, 614−620.
25. Kaplan, W., Hüsler, P., Klump, H., Erhardt, J., Sluis-Cremer, N., and Dirr, H. W. (1997) *Protein Sci. 6*, 399−406.
26. Wallace, L. A., Sluis-Cremer, N., and Dirr, H. W. (1998) *Biochemistry 37*, 5320−5328.
27. Wallace, L. A., Blatch, G. L., and Dirr, H. W. (1998) *Biochem. J. 336* (2), 413−418.
28. Stevens, J. M., Hornby, J. A. T., Armstrong, R. N., and Dirr, H. W. (1998) *Biochemistry 37*, 15534−15541.
29. Tradler, T., Stoller, G., Rucknagel, K. P., Schierhorn, A., Rahfeld, J., and Fischer, G. (1997) *FEBS Lett. 407*, 184−190.
30. Stenberg, G., Björnestedt, R., and Mannervik, B. (1992) *Protein Expression Purif. 3*, 80−84.
31. Weiner, M. P., Costa, G. L., Schoettlin, W., Cline, J., Mathur, E., and Bauer, J. C. (1994) *Gene 151*, 119−123.
32. Laemmli, U. K. (1970) *Nature (London) 227*, 680−685.
33. Habig, W. H., and Jakoby, W. B. (1981) *Methods Enzymol. 77*, 398−405.
34. Tonomura, B., Nakatani, H., Ohnishi, M., Yamaguchi-Ito, J., and Hiromi, K. (1978) *Anal. Biochem. 84*, 370−383.
35. Koppenol, W. H. (1980) *Biophys. J. 29*, 493−508.
36. Schreiber, G., and Fersht, A. R. (1996) *Nat. Struct. Biol. 3* (5), 427−431.
37. Etfink, M. R., and Ghiron, C. A. (1976) *Biochemistry 15*, 672−680.
38. Lehrer, S. S. (1971) *Biochemistry 10*, 3254−3263.
39. Ptitsyn, O. B., Pain, R. H., Semisotnov, G. V., Zerovnik, E., and Razgulyaev, O. I. (1990) *FEBS Lett. 262*, 20−24.
40. Semisotnov, G. V., Rodionova, N. A., Razgulyaev, O. I., Uversky, V. N., Gripas, A. F., and Gilmanshin, R. I. (1991) *Biopolymers 31*, 119−128.
41. Sinning, I., Kelywegt, G. J., Cowan, S. W., Reinemer, P., Dirr, H. W., Huber, R., Gilliland, G. L., Armstrong, R. N., Ji, X., Board, P. G., Olin, B., Mannervik, B., and Jones, T. A. (1993) *J. Mol. Biol. 232*, 192−212.
42. Wang, R. W., Newton, D. J., Johnson, A. R., Pickett, C. B., and Lu, A. Y. H. (1993) *J. Biol. Chem. 268*, 23981−23985.
43. Fischer, G., Bang, H., and Mech, C. (1984) *Biomed. Biochim. Acta 43*, 1101−111.
44. Xu, D., Tsai, C.-J., and Nussinov, R. (1998) *Protein Sci. 7*, 533−544.
45. Larsen, T. A., Olson, A. J., and Goodsell, D. S. (1998) *Structure 6*, 421−427.
46. Zhu, Z.-Y., and Karlin, S. (1996) *Proc. Natl. Acad. Sci. U.S.A. 93*, 8350−8355.
47. Hayes, J. D., and Wolf, C. R. (1988) *Glutathione Conjugation: Mechanisms and Biological Significance* (Sies, H., and Ketterer, B., Eds.) pp 316−356, Academic Press, London.
48. Kraulis, P. J. (1991) *J. Appl. Crystallog. 24*, 946−950.

BI991239Z